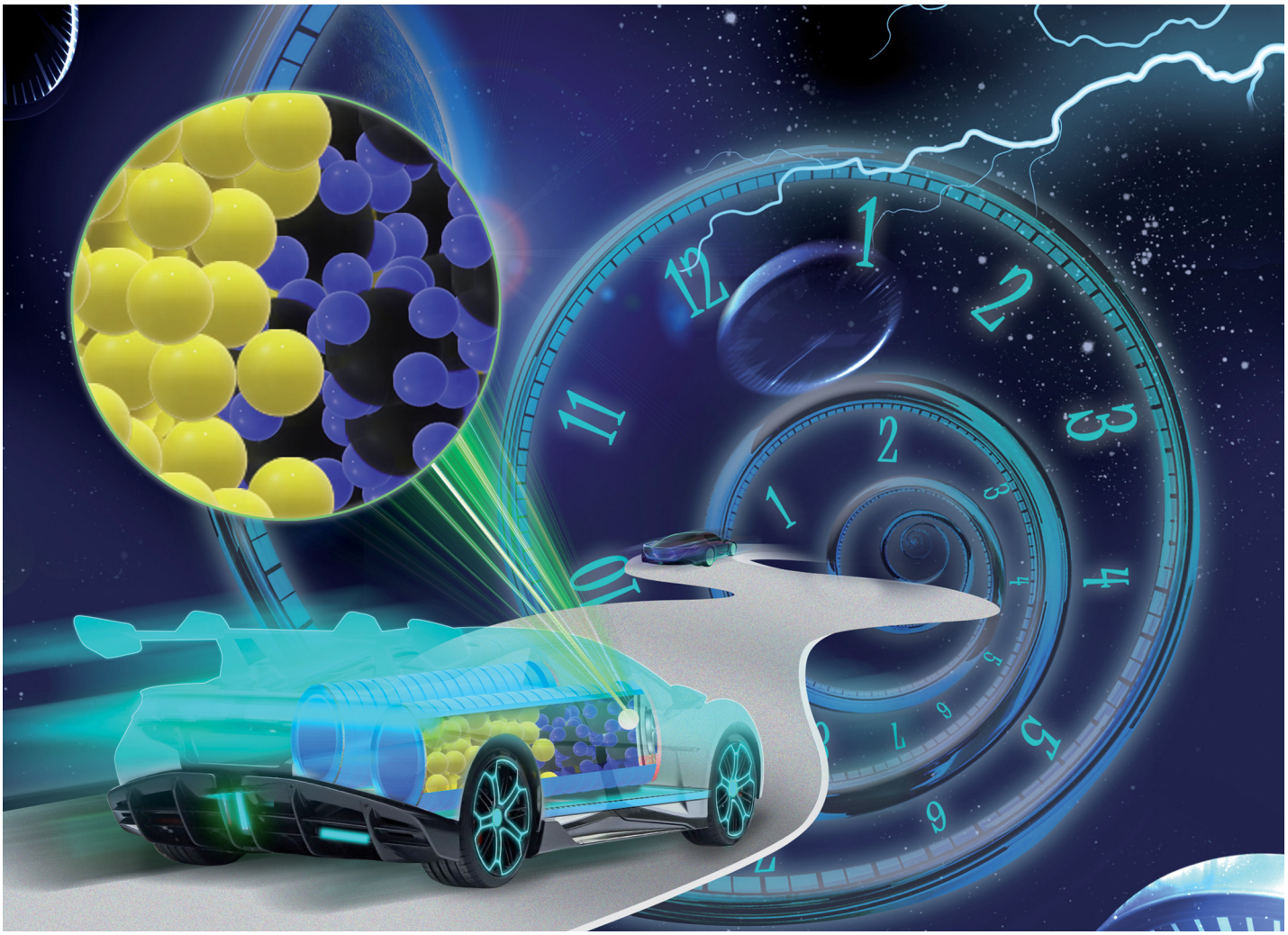

Highlighting a study by Dr Guang Yang's sulfide solid-state battery team in Energy Storage & Conversion Group, Chemical Sciences Division at Oak Ridge National Laboratory, US Department of Energy in close collaboration with Dr Jagjit Nanda's group at the SLAC-Stanford Battery Center, USA.

Effects of catholyte aging on high-nickel NMC cathodes in sulfide all-solid-state batteries

The catholyte's critical role in enhancing the calendar life of all-solid-state batteries highlights its impact on their longevity and efficiency.

As featured in:

See Jagjit Nanda, Guang Yang *et al.*, *Mater. Horiz.*, 2025, **12**, 119.

ROYAL SOCIETY OF CHEMISTRY

rsc.li/materials-horizons

Registered charity number: 207890

Materials Horizons

ROYAL SOCIETY OF CHEMISTRY

COMMUNICATION

View Article Online
View Journal | View Issue

Cite this: *Mater. Horiz.*, 2025, **12**, 119

Received 5th September 2024,
Accepted 24th October 2024

DOI: 10.1039/d4mh01211a

rsc.li/materials-horizons

Effects of catholyte aging on high-nickel NMC cathodes in sulfide all-solid-state batteries†

Yuanshun Li,[ab] Yukio Cho,[c] Jiyu Cai,[d] Chanho Kim,[a] Xueli Zheng,[c] Wenda Wu,[a] Amanda L. Musgrove,[a] Yifeng Su,[e] Robert L. Sacci,[a] Zonghai Chen,[d] Jagjit Nanda*[cf] and Guang Yang*[ag]

Sulfide solid-state electrolytes (SSEs) in all-solid-state batteries (SSBs) are recognized for their high ionic conductivity and inherent safety. The $LiNi_{0.8}Mn_{0.1}Co_{0.1}O_2$ (NMC811) cathode offers a high thermodynamic potential of approximately 3.8 V *vs.* Li/Li$^+$ and a theoretical specific capacity of 200 mA h g^{-1}. However, the practical utilization of NMC811 in sulfide SSBs faces significant interfacial challenges. The oxidation instability of sulfide solid electrolytes against NMC811 and the formation of the cathode electrolyte interphase (CEI) during cycling lead to degradation and reduced cell performance. Volumetric changes in NMC during lithiation and de-lithiation can also cause detachment from sulfide electrolytes or internal particle cracking. Despite extensive galvanostatic cycling studies to address the issues, the calendar life of sulfide SSBs remains poorly understood. Here, we systematically studied the effects of four different catholytes on the calendar aging of $LiNbO_3$ (LNO)-coated NMC811, including Li_6PS_5Cl (LPSCl), Li_3InCl_6–Li_6PS_5Cl (LIC–LPSCl), Li_3YCl_6–Li_6PS_5Cl (LYC–LPSCl), and $Li_{10}GeP_2S_{12}$ (LGPS). Our results indicate that LPSCl provides optimal capacity retention when stored at high state-of-charge (SOC) at room temperature, but the LIC–LPSCl cathode shows significant capacity degradation and chemical incompatibility. We also established an effective electrochemical calendar aging testing protocol to simulate daily usage, enabling quick inference of the calendar life of SSBs. This new testing approach accelerates materials selection strategies for high-nickel NMC composite cathodes in sulfide SSBs.

New concepts

Our investigation delves into the realm of calendar aging in sulfide all-solid-state batteries, specifically targeting NMC811 cathodes – a critically important yet largely unexplored area. A central and surprising finding from our research is that sulfide catholytes, typically considered less oxidatively stable than their halide counterparts, exhibit superior performance when used with lithium niobate-coated NMC811 cathodes. We thoroughly examine the interactions between high-nickel NMC811 cathodes and various catholytes, including Li_6PS_5Cl (LPSCl), Li_3InCl_6–Li_6PS_5Cl (LIC–LPSCl), and Li_3YCl_6–Li_6PS_5Cl (LYC–LPSCl), under simulated prolonged operational conditions. Among these, LPSCl demonstrates the most promising capacity retention, suggesting its potential to significantly enhance the longevity of sulfide-based solid-state batteries. Conversely, the LIC–LPSCl mixture shows considerable degradation due to chemical mismatches, adversely affecting cathode performance. We have introduced a robust electrochemical calendar aging testing protocol that provides a rapid and effective method for evaluating the long-term stability of cathode materials under realistic usage scenarios. These findings not only fill a crucial gap in existing literature but also introduce a conceptual advance by emphasizing the importance of catholyte selection in mitigating interface degradation and boosting the durability of sulfide all-solid-state batteries. This paradigm-shifting insight paves the way for future advancements in battery technology.

Introduction

Sulfide-based all-solid-state batteries (SSBs) present a highly promising alternative to lithium-ion batteries due to their comparable ionic conductivity and intrinsic safety in the operation of solid electrolytes. The development of nickel-rich $LiNi_xMn_{1-x-y}Co_yO_2$ (NMC, $x \geq 0.8$, $y \leq 0.1$) cathodes, such as NMC811, is critical to meeting high voltage and specific capacity requirements. NMC811 possesses a high thermodynamic potential of approximately 3.8 V *vs.* Li/Li$^+$. Additionally, NMC811 delivers a theoretical specific capacity of 200 mA h g^{-1},

[a] *Chemical Sciences Division, Oak Ridge National Laboratory, Oak Ridge, TN 37831, USA. E-mail: yangg@ornl.gov*
[b] *Department of Chemical and Biomolecular Engineering, The University of Tennessee Knoxville, Knoxville, TN 37996, USA*
[c] *Applied Energy Division, SLAC National Laboratory, Menlo Park, CA 94025, USA. E-mail: jnanda@slac.stanford.edu*
[d] *Chemical Sciences and Engineering Division, Argonne National Laboratory, Lemont, IL 60439, USA*
[e] *Materials Science and Technology Division, Oak Ridge National Laboratory, Oak Ridge, TN 37831, USA*
[f] *Department of Materials Science and Engineering, Stanford University, Stanford, CA 94305, USA*
[g] *The Bredesen Center for Interdisciplinary Research and Graduate Education, University of Tennessee Knoxville, Knoxville, TN 37996, USA*

† Electronic supplementary information (ESI) available. See DOI: https://doi.org/10.1039/d4mh01211a

outperforming $LiFePO_4$ at 170 mA h g^{-1}. Therefore, accelerating the development of NMC cathodes in sulfide SSBs is of great interest for urgent and broad energy storage applications.

The practical utilization of the NMC811 composite cathode in sulfide SSBs faces several critical interfacial challenges.[1] A major challenge is the oxidation instability of sulfide SSEs against NMC cathodes. Over cycling, the formation of the cathode electrolyte interphase (CEI) in the NMC composite cathode can lead to electrochemical and chemical degradation, resulting in a disconnected lithium-ion charge pathway and reduced cell performance.[2] Additionally, the volumetric change of NMC cathodes during lithiation and de-lithiation can either cause detachment from sulfide electrolytes or internal particle cracking, leading to a loss of active sites for capacity delivery.[3] Thus, considerable efforts have been devoted to increasing the capacity retention of sulfide SSBs by creating a stable CEI in the composite cathode. Two major strategies have been adopted and reported in the literature. The first one involves cathode surface coating, including using wet chemistry[4] with $LiNbO_3$ (LNO) or atomic layer deposition (ALD) with different oxide chemistries.[5] The second method is known as the bilayer design,[6] which engages halide electrolytes, such as Li_3InCl_6 (LIC) or Li_3YCl_6 (LYC), as a catholyte while retaining majority composition of sulfide SSEs as separators. This idea stems from the halide's broader electrochemical window, which improves the oxidation stability of the CEI. Numerous reports indicate that such bilayer sulfide SSBs can significantly improve capacity retention.[7–10]

Although galvanostatic cycling studies have been extensively performed on most sulfide SSBs to infer their performance and reliability, the calendar life of sulfide SSBs remains underexplored. Calendar life estimates a battery's lifespan from the point of manufacture, which depends solely on storage conditions and state of charge (SOC). Dubarry *et al.* initially developed calendar aging to study aging mechanisms in commercial Li-ion batteries.[11] They observed that the NMC cathode exhibits a significant degradation rate at 40 to 60 °C, whereas nickel–cobalt aluminum oxide (NCA) shows minimal change within the same temperature range. Similarly, it is crucial to measure the calendar life for next-generation batteries beyond lithium-ion technology. Xiao *et al.* emphasized that calendar life testing is mandatory for solid-state batteries to monitor minor interphase impedance growth rates.[12] This test reveals potential negative effects of SSE decomposition in response to high cathode loading and low SE loading in state-of-the-art designs. In a recent study, Kim *et al.* conducted a calendar aging test on NMC811-LIC|LIC/LPSCl|LiIn cells with different SOC aging protocols at 25 °C and 70 °C.[13] They demonstrated that this bilayer solid electrolyte with LIC as the catholyte protects NMC cathodes from significant capacity degradation when aged at high SOC for 7 days at 70 °C, compared to the high-capacity degradation observed at low SOC. However, very few calendar aging test protocols have been developed to study the aging mechanisms of sulfide SSBs. Similarly, there is a lack of systematic electrochemical experimental designs to standardize calendar aging tests and explore the effects of catholytes on the calendar life of NMC cathodes.

Herein, we adapted a calendar aging protocol developed for Li–Si batteries to explore sulfide SSBs.[14] We systematically studied the effects of four different catholytes on the calendar aging of the composite LNO-coated NMC811, including Li_6PS_5Cl (LPSCl), Li_3InCl_6–Li_6PS_5Cl (LIC–LPSCl), Li_3YCl_6–Li_6PS_5Cl (LYC–LPSCl), and $Li_{10}GeP_2S_{12}$ (LGPS). We demonstrated that LPSCl presents optimal capacity retention after aging when stored at high SOC at room temperature. The LIC–LPSCl cathode exhibits significant capacity degradation and chemical incompatibility, as confirmed by Raman imaging armed with the unsupervised learning algorithm, and sulfur K-edge XAS. Additionally, a robust electrochemical calendar aging testing protocol was developed to mimic daily use in mobile devices, enabling rapid estimation of the sulfide solid-state battery's calendar life over a short period (less than 10 days). The electrochemical calendar aging tests herein present a pivotal advancement in accelerating materials selection strategies for the development of high-nickel NMC composite cathodes for sulfide SSBs.

Results and discussion

To understand how catholytes impact the calendar life of NMC particles, an illustration of the aging protocol is presented in Fig. 1a. Originally, the calendar life aging protocol was developed for studying silicon's calendar life against liquid electrolytes in Si|NMC.[14] Briefly, the cell starts with three formation cycles at 0.1C from 1.98 V to 3.678 V against Li_xIn alloys. Then, it is held at 3.678 V for 180 hours to calendar age the NMC composite cathode. Following that, one diagnostic cycle is executed at 0.1C. Holding a battery at a full SOC simulates a practical condition when energy storage devices are routinely operated. For example, batteries in electric vehicles or phones are often 'overcharged,' with no minimum control applied to unplug a 100% SOC battery. It is believed that maintaining a high potential and overcharging a battery would accelerate side reactions at the electrode/electrolyte interphases, which are typically irreversible. This issue is even more critical in the cathode electrolyte interphase (CEI) of sulfide solid-state batteries. Four different catholytes were examined for their stability against LNO-NMC811 during calendar aging testing, including LPSCl, LGPS, LIC–LPSCl, and LYC–LPSCl. LPSCl was employed as a baseline catholyte. LGPS was reported to have the highest ionic conductivity in sulfide SSEs. LIC–LPSCl and LYC–LPSCl are two synergized halide and sulfide SSEs, representing advanced strategies that have been shown to effectively stabilize the CEI.[9,15]

The irreversible capacity loss after calendar aging is quantified through two means. One method involves comparing the discharge capacity from the last formation cycle (before aging) to that of the diagnostic cycle (after aging). This comparison directly reflects the effectiveness of the degradation of different catholytes against NMC cathodes. Fig. 1b reveals that the LPSCl-cathode reserves the highest discharge capacity after calendar aging at 122.97 mA h g^{-1} with a high 73.1% capacity retention. Similarly, LYC–LPSCl presents 106.34 mA h g^{-1}

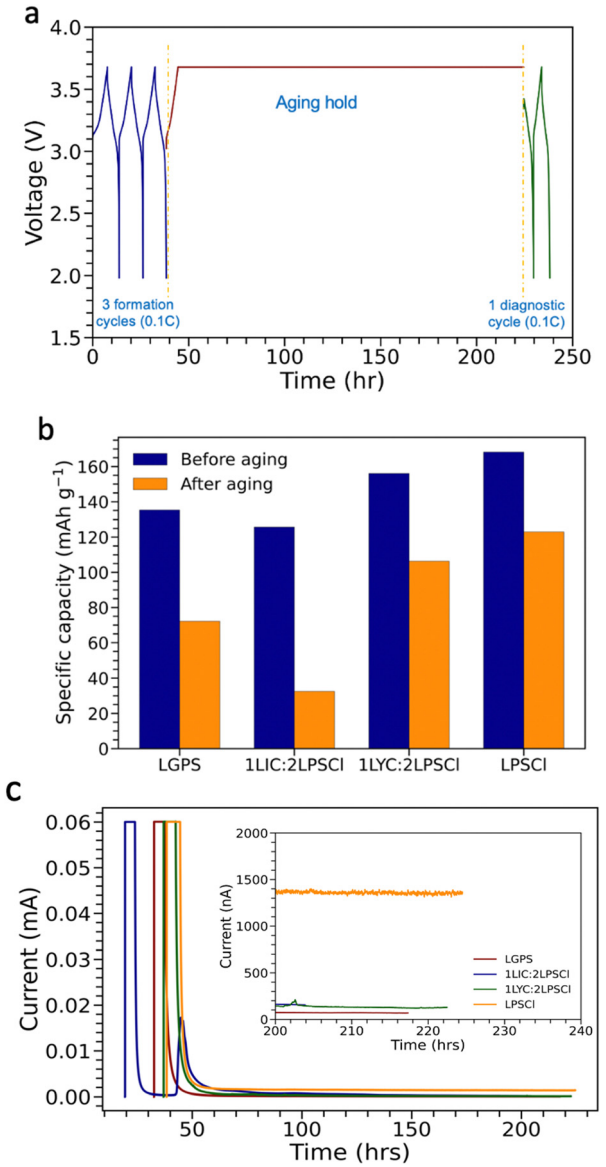

Fig. 1 Calendar life protocols and outcomes for Li_xIn|LPSCl|LNO-NMC811 SSB in different catholytes. (a) An illustration of calendar aging protocol by voltage holding[14,16] with direct modification applied to adjust for studying catholyte effects on calendar life of high Nickel NMC cathode in sulfide solid state battery. (b) Results comparing discharge capacities before and after calendar aging. (c) The leakage current as a function of time with nanoampere accuracy in 180 hours holding at 3.678 V (*vs.* Li_xIn or 4.3 V *vs.* Li/Li^+), with the specific zoom-in at the end of 20 hours of aging to distinguish the leakage current values among different catholytes.

(discharge capacity after aging) with 68.1% capacity retention. The LGPS-cathode presents a slightly lower capacity at 72.22 mA h g^{-1} and 53.3%. In contrast, the LIC–LPSCl cathode depicts significant degradation with only 25.8% capacity retention and 32.48 mA h g^{-1}. This indicates that curing the LIC–LPSCl cathode cell at high potential for one week resulted in severe irreversible capacity degradation, potentially attributed to catholyte decompositions. This LIC–LPSCl calendar life degradation effects on the cathode have the same influence on NMC622 as evidenced in Fig. S1 (ESI†). We have observed that for several years, researchers have been actively debating whether a bilayer LIC–LPSCl is necessary, or if LIC alone should replace LPSCl as a catholyte to safeguard the NMC cathode. Ye *et al.* reported that LIC serves as a catholyte, and using LPSCl as a solid electrolyte enhances pellet type SSB performance in both discharging capacity and capacity retention.[17] In contrast, Carolin *et al.* reported chemical incompatibility between LIC and LPSCl, which does not benefit the overall electrochemical performance when introducing LIC as a catholyte.[18] The aging test underscores that storing cells at a high state of charge (SOC) with LIC–LPSCl blended catholyte is not recommended. The potential mechanisms behind this recommendation are further elucidated in subsequent characterizations.

The second calendar aging quantification method involved monitoring the residual current during high voltage holding, as shown in Fig. 1c. It is assumed that the cell is fully charged and only side reaction due to SSE oxidative decomposition occurs at 3.678 V approaching to the end of the 180 hours holding period. In the first 20 hours of voltage holding, the current drops significantly, which corresponds to compensating for the 'unfinished' de-lithiation process in the cathode. Furthermore, the residual current stabilizes and reaches a plateau during continuous high voltage holding. At the end of voltage holding, the zoom-in profile was revealed to further investigate the steady-state residual current, which is assigned to the side-reaction rate. The orange noisy curve referred to the residual current between LPSCl and NMC811, registering at 1400 nA, depicts that the LPSCl-cathode undergoes the severest side reaction compared with other catholytes. Blending LIC or LYC with LPSCl yields almost identical residual current responses at approximately 170 nA. This suggests that blending LIC or LYC with LPSCl could stabilize the interphases of Li_xIn|NMC and reduce the residual current. Additionally, the LGPS-cathode presents the lowest value of 80 nA. A possible explanation is that LGPS can mitigate the interfacial side reaction by lowering its parasitic electron transfer across the interphase. During the voltage holding process, the vacancy of lithium ion in NMC reaches maximum. Thus, LGPS with its Ge substituted stable structure and low Young's modulus exhibits better stability against NMC with minimal lithium existing in the CEI. However, obviously, the findings from the second method are not consistent with the first method. Specifically, the LPSCl exhibits the best aging capacity retention, but it produces the highest residual current during aging. Several possible factors can contribute to this discrepancy: (1) The Li_xIn alloy has a fluctuating voltage response during the lithiation process, causing the holding voltage to be inaccurate as the upper cutoff voltage; (2) different catholytes can form different CEIs, affecting their stability in response to high voltage. This underscores the limitations of the second method, highlighting areas that require further refinement.

When reaching the voltage plateau during lithiation, Li_xIn alloy resides at 0.62 V *vs.* Li/Li^+, lower than the reduction decomposition of the sulfide SSE. To delineate the sulfide SSE reduction decomposition at the anode surface during voltage holding, the $Li_4Ti_5O_{12}$ (LTO) was further chosen as the counter electrode to evaluate the leakage current in a specific study of catholytes aging effects. In addition, LTO has

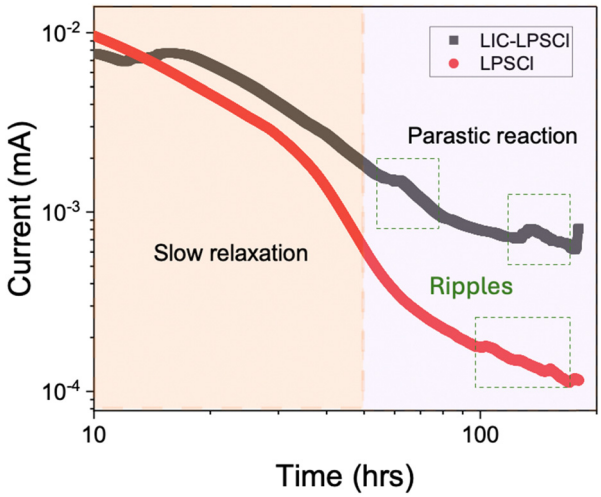

Fig. 2 The leakage current response of the LTO|LPSCl|NMC811 full cell over 180 hour of voltage holding (a light orange dashed line delineates major distinct electrochemical reactions, hypothesized to occur due to different leakage current responses). Two reactions are assumed during the voltage holding process: (1) slow relaxation of NMC to reach equilibrium; (2) parasitic reaction. Notable fluctuations are highlighted within green dashed boxes, indicating the additional relaxation reaction for probably more interfacial contact of electrode materials.

a flat voltage plateau above 1.5 V *vs.* Li/Li^+, minimizing the reduction decomposition of the SSE at anode surface. In this case, the leakage current is more representative to the oxidation parasitic reactions, after the electrode reaches to its equilibrium state. LTO|LPSCl|NMC full cell with two representative catholytes (LPSCl, LIC–LPSCl) was tested in the same calendar protocol above with adjusting the cut-off voltage to 2.75 V exclusively because LTO has a potential at 1.55 V *vs.* Li/Li^+. The difference of leakage currents between two catholytes looks obvious in Fig. 2, suggesting much higher rate of parasitic reactions using LIC–LPSCl catholyte. This is aligned with the most significant capacity degradation observed in LIC–LPSCl previously after aging. Thus, we demonstrate the LTO anode as an effective counter electrode in measuring leakage current accounting for the cathode side oxidation parasitic reaction in a sulfide all-solid-state cell. However, additional research is required to develop a quantitative model that accurately predicts the state of health of solid-state batteries (SSBs) based on their calendar aging behavior.

Furthermore, we also noticed some ripples occurred particularly in LIC–LPSCl (Fig. 2). The abruptly increased leakage current is very likely due to the sudden increase of interface contact between cathode and catholyte to facilitate parasitic reactions, or due to the transitionally accelerated side reactions. Considering the mechanical nature of more rigid LIC than LPSCl, the catholyte using LIC–LPSCl potentially suffers worse contact with NMC under the same cell stack pressure. On the other hand, LPSCl current response also depicts at least two different reactions. The first reaction before 50 hours is suspected to be the slow relaxation of the concentration gradient in the NMC, while it is typically completed within first few hours in the liquid cells as evidenced in many previous reports.[19,20] However, SSBs suffer poor and less covered interface contact at cathode compared with a liquid electrolyte lithium-ion battery. Thus, SSBs, owing to their sluggish ion transport, typically require a longer time to reach the equilibrium during the voltage holding. Additionally, the later reaction after 50 hours is referred to parasitic reaction, and some ripples were also detected. These can be explained by the new formations of side products during the parasitic reaction, contributing to dramatically changing the volume. This induces fluctuation of interfacial contact during the voltage holding, randomly facilitating parasitic reaction.

To further elucidate how interfacial resistance changes during calendar aging testing, *in situ* electrochemical impedance spectroscopy (EIS) was performed to measure the impedance in three states: pristine, before aging, and after aging. Similar EIS evolution trends were observed for four catholytes shown in Fig. 3. Briefly, starting with the pristine state, the EIS exhibits a semi-circle followed by a straight tail. The resistance value at the junction between the semi-circle and the long tail directly reflects the bulk resistance, R_1. As shown in the four plots, after three formation cycles, the bulk resistance of the cell decreases due to the consolidation of solid electrolytes over cycling. After high voltage holding, it is believed that interphases are formed, contributing to the second semi-circle present in the Nyquist plot. By comparing the three states, we aim to identify which step is limiting in different catholytes.

LPSCl cathodes exhibit the best performance with the lowest interfacial resistance post-aging, while LIC–LPSCl cathodes show the highest resistance and electrochemical instability at all stages, indicating chemical incompatibility explored further with advanced spectroscopy. Fig. 3a and d depict that LPSCl- and LGPS-cathodes present similar initial bulk resistance, registered at 300 ohms, superior to the LIC–LPSCl-cathode's 350 ohms (shown in Fig. 3b) but less effective than the LYC–LPSCl-cathode, which registers at 250 ohms (Fig. 3c). After three formation cycles, the LPSCl-, LGPS-, and LYC–LPSCl-cathodes demonstrate reduced bulk resistances of 100 ohms, contracting with only a modest reduction to 300 ohms for the LIC–LPSCl cathode. Upon aging, the LPSCl cathode significantly outperforms all other catholytes, maintaining an interfacial resistance of approximately 300 ohms.

Notably, the interfacial resistance of the LIC–LPSCl cathode is about 300% greater than that of LPSCl, 250% more than LYC–LPSCl, and 200% higher than LGPS. Additionally, the post-aging phase reveals that the LGPS cathode exhibits a higher interfacial resistance compared to the LPSCl cathode, despite presenting a lower leakage current, suggesting distinct interfacial side reaction pathways or mechanisms compared to LPSCl. Furthermore, our findings confirm the electrochemical disfavor of the LIC–LPSCl cathode at all stages of the calendar aging test, corroborating earlier observations of significant capacity degradation. This is supported by previous reports of chemical incompatibility between LIC and LPSCl,[18,21] prompting further investigation into this issue through Raman mapping and XAS (Ni K-edge and sulfur K-edge) analyses.

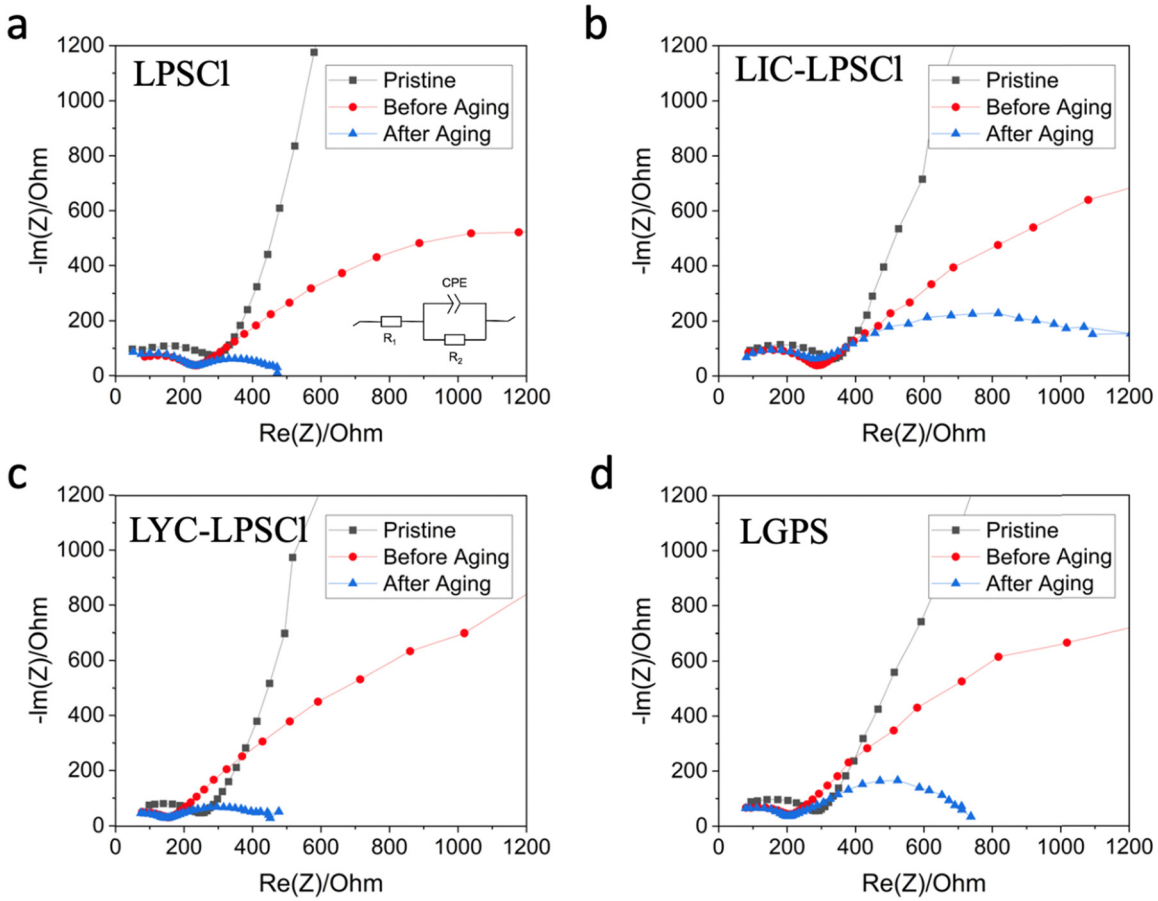

Fig. 3 EIS Nyquist plot for four different catholytes of (a) LPSCl, (b) LIC–LPSCl, (c) LYC–LPSCl, (d) LGPS. The inlet of (a) includes the equivalent circuit model, with R_1 representing bulk SSE resistance, R_2 representing interfacial resistance, and CPE presenting the constant phase element.

To explore the chemical and structural changes of CEI of post-aging electrodes, Raman spectroscopy was employed for mapping and analyzed using K-means clustering. Four post-aging samples were meticulously stripped with an insulating ceramic knife to expose the cathode in a plane view as shown in Fig. S2 (ESI†). Fig. 4a, d, g, and j present five distinct clusters, representing possible compositional variations in the cathode. The Raman shift ranges from 350 to 550 cm^{-1}, indicating the P–S stretching. Notably, a peak at 422 cm^{-1} indicative of a classical PS_4^{3-} was observed across all cathodes but varied locally due to environmental effects. Furthermore, the signal of the peak was normalized to the highest intensity to enhance the differentiation of the concentration of the 'new peak'. To examine the potential new substances or chemicals manifesting as new Raman peaks, we performed single Raman spectral analysis for the pristine cathode with different catholytes as a reference, as depicted in Fig. S3 (ESI†). Our findings reveal that blending LIC or LYC with LPSCl does not yield new peaks other than PS_4^{3-}. However, as illustrated in Fig. 4d, a peak at 460.8 cm^{-1} emerges on the LIC–LPSCl-cathode after aging, suggesting the formation of a new side product in the CEI. This peak is attributed to the S–S bond in molten/polymerized elemental sulfur.[22,23] This observation underscores the chemical incompatibility between LIC and LPSCl, particularly when the cell is stored at a high SOC. Additionally, Fig. 4b, e, h, and k reveal markedly heterogeneous CEIs, highlighting the complexity of reactions occurring within the cathodes. Moreover, the composition of each colored cluster was statistically analyzed in Fig. 4c, f, i and l, enabling further quantification of clusters rich in LPSCl-rich or sulfur. For example, in the LIC–LPSCl-cathode, clusters 2, 3, and 5 account for sulfur-rich regions, and their total percentage is over 50%, indicating significant degradation and sulfur enrichment within half of the CEI.

To determine the electrochemical stability of nickel in the composite NMC811 cathode with different catholytes after 180 hours of voltage holding, we performed Ni K-edge XANES and EXAFS on post calendar aging samples. As shown in Fig. 5a, the spectral shape of four aged samples with different catholytes exhibits remarkable similarity to the reference pristine LPSCl-NMC spectrum. This similarity suggests the absence of macroscopic decomposition or phase changes in the NMC during high voltage holding. The first derivative of the XANES spectra enables a clear comparison of the nickel oxidation states across all the samples. Notably, the LIC–LPSCl-cathode (at 8343.8 eV) exhibits an oxidation state around 1 eV higher than the other cathode counterparts (from 8342.4 to 8342.7 eV). This higher oxidation state suggests a greater degree of irreversible changes in the nickel of the LIC–LPSCL-cathode after

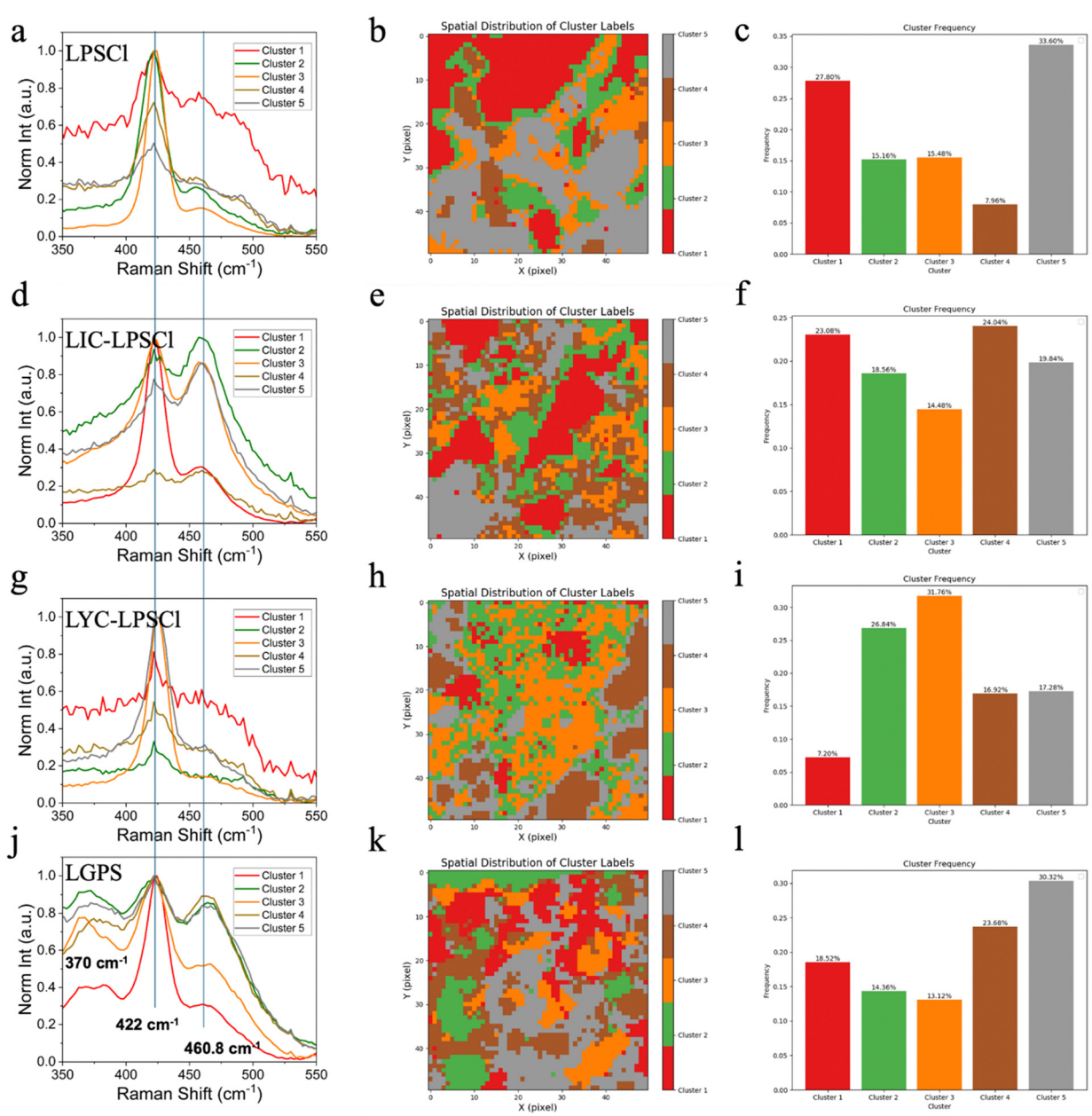

Fig. 4 Comprehensive Raman spectral analysis through K-means clustering and spatial clustering distribution of different cathodes. Panels (a), (d), (g) and (j) display normalized Raman spectra for LPSCl, LIC–LPSCl, LYC–LPSCl, and LGPS cathodes, respectively, indicating distinct peaks corresponding to varied clusters. Panels (b), (e), (h) and (k) depict the spatial distribution of cluster labels within the cathodes, analyzed using machine learning with K-means clustering. Panels (c), (f), (i) and (l) present the frequency of each cluster, showcasing the predominance or rarity of specific Raman features across the cathode types.

calendar aging, consistent with the notably lower capacity retention observed in the electrochemical exploration. Despite all cathodes being maintained in a discharged state at completion, an imbalance in lithium levels relative to the pristine state persists. Consequently, the Ni oxidation state in aged samples is elevated compared to the pristine NMC (8341.7 eV). Fourier transform EXAFS analysis of Ni-K edge across all cathodes reveals a consistent first peak at around 1.5 Å, corresponding to Ni–O first shell coordination, and a second peak at around 2.5 Å is ascribed to Ni–M (M = Ni, Mn and Co) scatterings. Comparisons with the pristine reference (shown in Fig. 5c) disclose no significant changes in bond distances, suggesting the stability of the NMC phase during high voltage holding.[24,25]

To support the findings from Ni K-edge analysis, we further performed XRD on both LPSCl and LIC–LPSCl samples before and after calendar aging, as shown in Fig. S4 and S5 (ESI†). Pristine LPSCl *vs.* aged LPSCl were analyzed as a control to aid in the identification of NMC811 peaks for the cathode before *vs.*

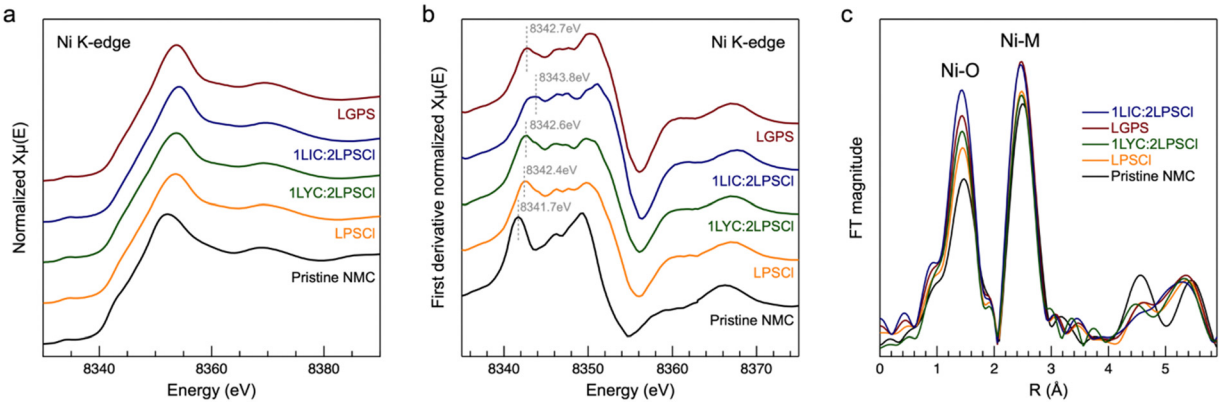

Fig. 5 (a) Normalized XANES spectra at Ni K-edge for pristine LPSCl–NMC811, aged cathode samples with different catholytes among LPSCl, LGPS, LYC–LPSCl, LIC–LPSCl (note that Ni XAS were collected from peeled off current collector, from the residue NMC on it, and also all cathodes are in discharged condition); (b) First derivative of XANES spectrum at Ni K-edge highlights oxidation difference among all catholytes; (c) FT-EXAFS spectra in *R* space at Ni K-edge exhibits moderate changes in Ni local structure.

after calendar aging. NMC811 peaks were confirmed *via* Mo to Cu 2θ conversion and compared to a previously reported diffractogram (ICSD #8362, peak assignment for NMC811 summary can be accessed in Table S1, ESI†).[26] 0.1° peak shifts are observed for both LPSCl and NMC811 after cycling which suggests lithiation into the layered structure, causing slight lattice expansion. Additionally, a notable decrease in intensity is observed for all peaks corresponding to NMC 811 after aging. For peaks at higher 2θ values, such as the NMC 811 peak corresponding to (105) at 21.8° (Fig. S6, ESI†), the peak is absent after cycling. This overall decrease in peak intensity corresponds to a decrease in crystallinity over the course of calendar aging. Similar observations have been previously reported in the literature.[27]

To elucidate the interfacial side reaction mechanisms between catholytes and the NMC811 cathode, we conducted sulfur K-edge XAS analyses on aged LPSCl and LIC–LPSCl aged samples. Notably, the LIC–LPSCl sample presents a distinctively different sulfur chemistry compared to other LPSCl samples (Fig. 6a). This indicates that most of the sulfur in the LIC–LPSCl sample is oxidized to the level of elemental sulfur. This observation corroborates our Raman mapping results, which identified sulfur as the primary side product in aged LIC–LPSCl samples, contributing to the limited capacity retention following the high voltage holding. Furthermore, XPS spectra for S 2p and P 2p orbitals in these samples indicate that the sulfur and phosphorus species of LPSCl degraded to P_2S_x, similar to what has been reported in literature[28–30] (Fitting parameters are provided in Tables S2 and S3, ESI†). The LIC–LPSCl catholyte undergoes significant decomposition to sulfur, Li_2S, and Li_3P (Fig. 6b and c). This degradation is likely driven by LIC's catalytic effect during high voltage holding, leading to irreversible decomposition and substantial cathode volume changes. These changes result in the NMC losing contact and being locked in a high oxidation state.

Our findings suggest that the poor capacity retention in LIC–LPSCl over calendar aging is due to the formation of parasitic products, such as elemental sulfur, and species containing a higher irreversible oxidation state of nickel. However, it remains uncertain whether this substantial capacity degradation

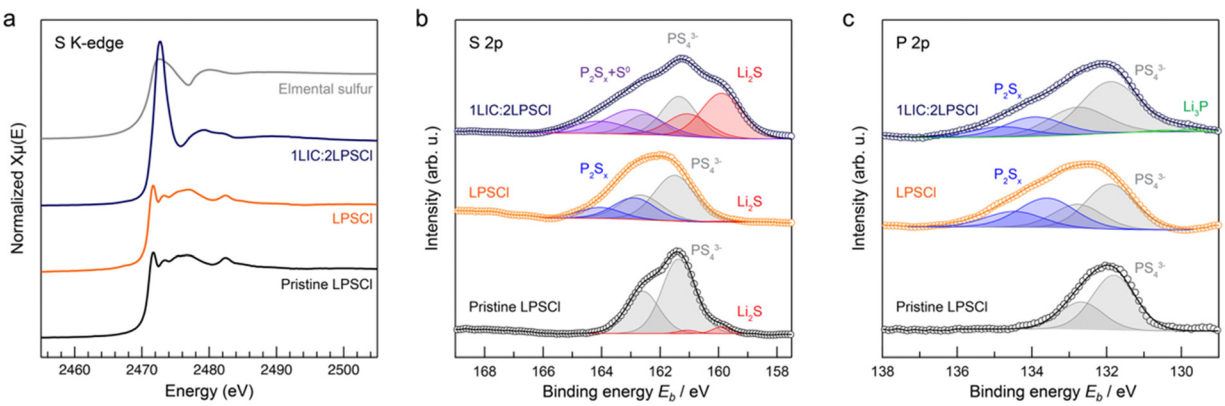

Fig. 6 (a) Normalized XANES spectra at the S K-edge for pristine LPSCl- NMC811, aged NMC811 with LPSCl and LIC–LPSCl catholytes, and elemental sulfur as a control. (note that S XAS data were collected from the cycled cell); XPS spectra of (b) the S 2p, and (c) the P 2p orbitals for pristine LPSCl, aged LPSCl catholyte and LIC–LPSCl catholyte, illustrating the decomposition pathway of LIC–LPSCl.

is solely attributed to chemical and structural changes of CEI. To further investigate this, we performed scanning electron microscopy with energy-dispersive X-ray spectroscopy (SEM-EDX) to investigate the morphological change in NMC particles within LPSCl and LIC–LPSCl.

Notably, Fig. 7b reveals that the LIC–LPSCl cathode presents internal cracks of NMC and voids between the NMC particle and LIC–LPSCl electrolyte after aging, which likely contribute to capacity degradation due to the internal cracking of particles and loss of contact with the catholyte and VGCF. In contrast, the LPSCl cathode demonstrates that the NMC particle remains intact with minimal internal microcracking (Fig. 7a). To further justify the different mechanical behaviors of the CEI when using different catholytes, we also included lower magnification SEM images of the aged LPSC-cathode and LIC–LPSCl-cathode in Fig. S7(a) and (b) (ESI†). We found that the LPSCl cathode presents a more homogeneous material distribution compared to the LIC–LPSCl cathode, indicating less volume change and detachment in the LPSCl-cathode during high voltage holding. Previous EIS measurement (Fig. 3a and b) also underscores a significant difference in interfacial resistance between the LPSCl cathode and LIC–LPSCl cathode after aging. This suggests that the impedance growth in the LIC–LPSCl cathode interphase is likely attributed to the formation of the elemental sulfur. The insulative S formation, together with the physical contact loss, impedes lithium-ion transport between the NMC811 and the catholyte. These observations provide additional evidence that catholyte effects significantly influence the chemical and structural integrity of the cathode, as well as its mechanical stability.

Scheme 1 is presented below to highlight the key different chemical compositions on the CEI after aging between LPSCl and LIC–LPSCl samples. The catholytes play a vital role in its calendar aging performance on the NMC. Highly oxidized elemental sulfur was detected as the major side product in the interphase. The higher oxidative state of Ni was also detected in aged LIC–LPSCl cathode in comparison to LPSCl-cathode. It has been reported that highly oxidized or fully charged Ni^{4+} tends to react with electrolyte and facilitates parasitic reaction.[27]

To enhance NMC811 aging performance, two main strategies were explored: (1) using single crystal NMC and (2) optimizing charge/discharge conditions. Our preliminary results (Fig. S8(a) and (b), ESI†) show that both approaches – using single crystal NMC811 and reducing the c-rate during the formation cycle – effectively improve aging performance, as indicated by higher capacity retention and lower leakage current. Further investigation into their mechanisms is planned for future studies.

Experimental

LPSCl solid electrolyte thin film fabrication

The protocol for the fabrication of the LPSCl thin film was developed by our group and its step-by-step details can be accessed in ref. 31. Binder solution was firstly prepared by mixing 1270 kg mol^{-1} poly(isobutylene) (PIB) (Scientific Polymer Products, Inc., New York, U.S.), toluene, and two stirring bar. The stock binder solution is controlled in 7.4 wt% PIB. The LPSCl slurry was prepared by mixing as-obtained LPSCl (3–5 μm; NEI Corp., New Jersey, U.S.), stock binder solution, and toluene with a solvent to solid ratio of 1 : 1 in a glass vial. Then, three zirconia milling media were added into the vial and rolled overnight in a flat roller machine. The slurry was carefully distributed in a

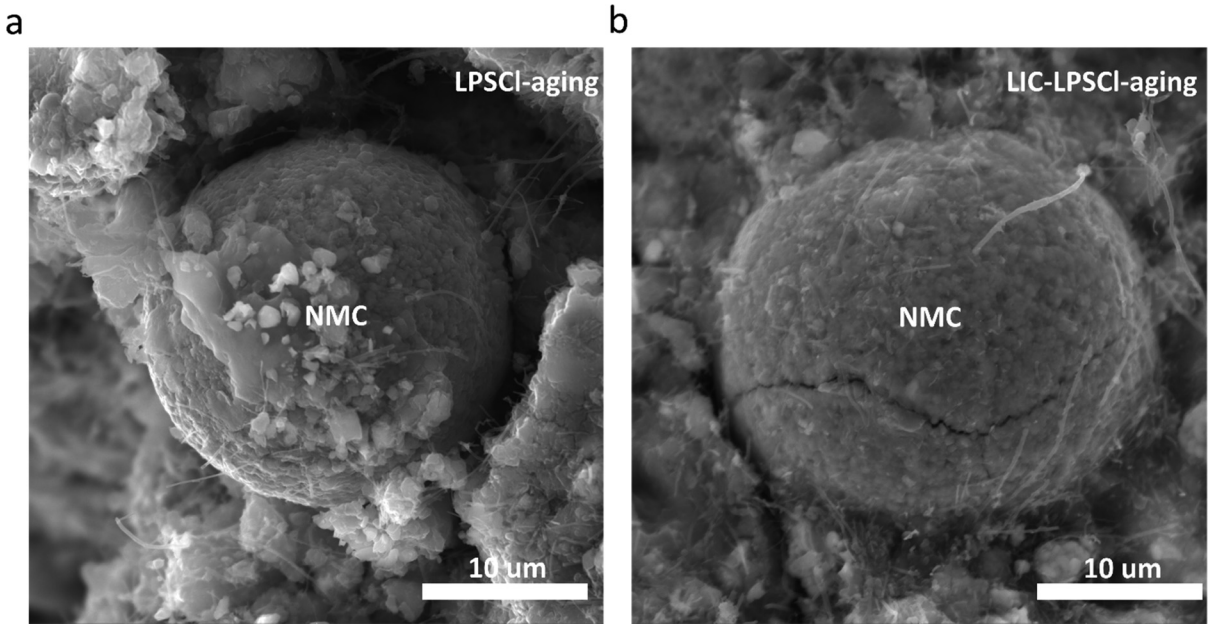

Fig. 7 SEM micrographs displaying the morphological changes in cathodes after aging in various catholyte environments. (a) NMC particles aged in LPSCl; (b) NMC particles aged in LIC–LPSCl, exhibiting internal cracking.

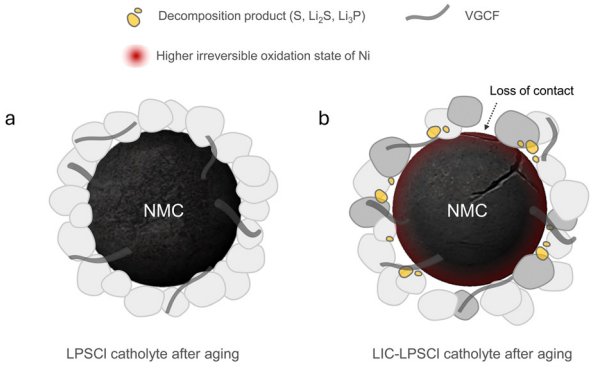

Scheme 1 An illustration to elucidate the difference in CEI and interface evolution of NMC811 after calendar aging process.

pre-dried meta film, following by 8 mil (200 μm) doctor blade casting. Well-casted LPSCl was dried in the large anti-chamber overnight. The LPSCl thin film was obtained by calendaring the deposited and dried LPSCl between two mylar films to detach LPSCl. The thickness of the calendar machine was fixed at 304 μm, and multiple calendaring process was needed to achieve the desired thickness of the thin film and free-standing film was obtained. All calendar processes were performed under room temperature (cold pressing).

LIC and LYC synthesis

Li_3InCl_6 was synthesized by first fully dissolving LiCl and $InCl_3$ (>99.99%, Sigma-Aldrich) in a 3 : 1 molar ratio in DI water. The solution was sonicated to deaerate then the bulk water was removed using a rotovap at 40 °C. The flask was quickly transferred to an Argon filled glovebox to limit continued exposure to moisture. We ground the precipitate by hand with a mortar and pestle and dried the powder at 80 °C in a vacuum overnight. Li_3YCl_6 was synthesized similarly but with the addition of 3 molar equivalents of ammonium chloride to the aqueous solution. Again, the solution was sonicated, then dried using a rotovap at 80 °C followed by drying at 150 °C overnight. The sample was hand ground then pelletize and heated to 500 °C (heating rate 5 °C min^{-1}) for 5 h under an argon flow (30 mL min^{-1}). Both samples showed less than 5% by wt LiCl.

Composite electrode preparation

The composite NMC cathode was prepared by mixing $LiNbO_3$-coated NMC811 active material acquired from NEI Corp. with manufactured standard specification of $D_{50} \sim 12$ μm in Fig. S9 (ESI†) (the thickness of the $LiNbO_3$ coating was unveiled using TEM and it is roughly 15 nm, as shown in Fig. S10, ESI†), various catholytes (LPSCl, LIC–LPSCl, LYC–LPSCl, and LGPS), and vapor grown carbon fiber (VGCF) at a weight ratio of 60 : 35 : 5 inside an argon-filled glovebox. Zirconia milling medium was added to the mixture in a weight ratio of 5 : 1 relative to the composite mass. The sealed mixture was then dry-milled using a Turbula mixer for one hour.

The composite LTO anode was prepared by mixing the $Li_4Ti_5O_{12}$ active material, LPSCl, and VGCF in a weight ratio of 60 : 30 : 10 in an Ar-filled glovebox. The zirconia milling medium was added to the mixture in a weight ratio of 5 : 1 relative to the composite mass. The sealed mixture was then dry-milled using a SPEX mixer for 5 min.

Battery assembly and electrochemical testing

Cell tests were conducted at room temperature using PEEK cells with a diameter of 6 mm. Two electrolyte sheets, each 6 mm in diameter, were placed in a mold and pressed at 20 bar to form the LPSCl layer. Subsequently, the cathode composite was spread on one surface, followed by placing carbon-coated Al foil as the current collector. This assembly was cold pressed at 60 bar for 3 minutes. Subsequently, a 5 mm diameter indium foil (150 × 150 TF, custom thermoelectric) and a 6 mm diameter copper foil were added on the opposite side of the electrolyte layer. The stack was then secured by tightening to achieve a stack pressure of 50 MPa roughly.

The galvanostatic tests were conducted between 1.98 V and 3.678 V *vs.* Li_xIn to examine the characteristics of different catholytes. The electrochemical impedance spectra (EIS) were obtained under open circuit conditions with an amplitude of 20 mV from 1 MHz to 100 mHz. Electrochemical evaluations and current leakage monitoring during the charged state were performed using Biologic EC-Lab software. All fabrication processes and electrochemical evaluations were carried out within an argon-filled glovebox.

Raman mapping

Raman mapping was performed using a Horiba XploRA confocal Raman system. This system is equipped with a 405 nm UV laser, and the laser power was meticulously controlled to be below 500 μW to prevent sample damage. The mapping was conducted at 50× magnification, maintaining a spot size of 1 μm to ensure spatial resolution. Data were collected using a diffraction grating with 2400 grooves per mm. The mapping covered an area of 50 by 50 points, resulting in a total analysis of 2500 points. All Raman analysis results were processed and analyzed using the Horiba Labspec 6 imaging and spectroscopy tool.

SEM-EDX

Materials were characterized using a TESCAN model MIRA3 scanning electron microscopy (SEM) equipped with an EDAX Octane Elect Super Silicon Drift Detector. We operated at 20 kV for microstructure characterization and X-ray-based chemistry analysis. We used the secondary electron (SE) mode to obtain microstructure images, and for analyzing chemical compositions, we utilized energy dispersive spectroscopy (EDS).

TEM

The TEM imaging was performed using a JEOL JEM-2100F equipped with a Schottky field emission gun operated at 200 kV.

XAS

Ni K-edge XANES and EXAFS spectra were collected using fluorescence mode at the beamline 4–1 of the Stanford Synchrotron

Radiation Light source (SSRL). Metallic nickel foil was used as reference and a Si(220) crystal was used as a monochromator. S K-edge XANES spectra are collected using the fluorescence mode at the beamline 4–3 of SSRL. Si(111) double-crystal monochromator was used with the cutoff energy of the upstream bare silicon mirror set below 6 keV to reject harmonics. To minimize atmospheric attenuation of the X-rays, the experiment was conducted in an atmosphere of helium gas. All data were analyzed using Athena.

XPS

XPS was performed using a PHI Versaprobe 3 with an Al Kα source radiation of 1486.6 eV. Spot size was set to 200 μm and pass energy was set to 55 eV. CasaXPS software was employed to fit the XPS core level spectra, with peak calibration being performed with respect to the C 1s peak (284.8 eV).

XRD

XRD was performed using a Rigaku SmartLab diffractometer with a Mo Kα X-ray source (0.71 Å). All samples were prepared using a sealed air-tight sample holder under an inert atmosphere to preserve the samples during data collection. Diffractograms were collected from 5° to 40° at a scan rate of 0.7° min^{-1}. Diffractograms of LPSCl before and after cycling were collected to aid in NMC 811 peak identification. A Mo to Cu 2θ conversion was done for all NMC 811 peaks to compare to ICSD #8362 for phase confirmation.

Conclusion

In this study, we systematically explored the impact of various catholytes on the calendar aging of NMC811 in sulfide SSBs, highlighting the crucial role played by catholyte composition in determining the electrochemical performance and durability of high-nickel NMC cathodes. Our comprehensive electrochemical evaluations, combined with advanced spectroscopic and imaging analyses, reveal that while the LPSCl catholyte offers superior capacity retention and stability, the LIC–LPSCl blend exhibits significant degradation, emphasizing the detrimental effects of catholyte incompatibility on cell longevity.

The data convincingly demonstrate that blending LIC with LPSCl accelerates interfacial side reactions and capacity degradation during calendar aging, underscoring the need for careful selection and optimization of catholyte materials in the design of SSBs. The profound impact of LIC–LPSCl on the electrochemical stability of NMC811, particularly in terms of irreversible nickel oxidation and the formation of parasitic sulfur species, calls for a reevaluation of current strategies employing mixed catholyte systems. Given the pressing demand for reliable and durable energy storage solutions, our findings stress the importance of further research into catholyte compositions that can enhance the interfacial stability and extend the operational life of sulfide SSBs. We note that future studies should focus on the development of novel catholyte materials that can withstand high operational voltages and resist chemical decomposition, potentially through the incorporation of new halide and sulfide formulations or innovative coating technologies. Ultimately, the insights gained from this work not only contribute to a deeper understanding of the degradation mechanisms in high-nickel cathode materials but also pave the way for the next generation of all-solid-state battery technologies. By advancing our knowledge of catholyte–cathode interactions and their implications on battery performance, we move closer to achieving the high-capacity, long-life batteries needed for future energy storage applications.

Data availability

The data supporting this article have been included as part of the ESI.†

Conflicts of interest

There are no conflicts to declare.

Acknowledgements

This research was conducted at the Oak Ridge National Laboratory, managed by UT Battelle, LLC for the U.S. Department of Energy (DOE) and is sponsored by the Office of Energy Efficiency and Renewable Energy (EERE) in the Vehicle Technologies Office (VTO) through the Advanced Battery Materials Research (BMR) Program, managed by Drs Simon Thompson and Tien Duong. This manuscript has been authored by UT-Battelle, LLC under Contract No. DE-AC05-00OR22725 with the U.S. Department of Energy. SEM and EDX research were conducted as part of a user project at the Center for Nanophase Materials Sciences (CNMS), which is a US Department of Energy, Office of Science User Facility at Oak Ridge National Laboratory. XPS was performed at the Stanford Nano Shared Facilities (SNSF), supported by the National Science Foundation under award ECCS-2026822. The use of the Stanford Synchrotron Radiation Lightsource at SLAC National Accelerator Laboratory is supported by the U.S. Department of Energy, Office of Science, Office of Basic Energy Sciences under Contract No. DE-AC02-76SF00515. Y. C. was supported by the Japan Society for the Promotion of Science (JSPS) overseas research fellowship and the Stanford Energy Postdoctoral Fellowship and the Precourt Institute for Energy.

References

1 T. Brahmbhatt, G. Yang, E. Self and J. Nanda, Cathode–Sulfide Solid Electrolyte Interfacial Instability: Challenges and Solutions, *Front. Energy Res.*, 2020, **8**, 570754.
2 Y.-W. Byeon and H. Kim, Review on Interface and Interphase Issues in Sulfide Solid-State Electrolytes for All-Solid-State Li-Metal Batteries, *Electrochem.*, 2021, 452–471.
3 T. Shi, Y.-Q. Zhang, Q. Tu, Y. Wang, M. C. Scott and G. Ceder, Characterization of mechanical degradation in an all-solid-state battery cathode, *J. Mater. Chem. A*, 2020, **8**(34), 17399–17404.

4 X. Li, L. Jin, D. Song, H. Zhang, X. Shi, Z. Wang, L. Zhang and L. Zhu, $LiNbO_3$-coated $LiNi_{0.8}Co_{0.1}Mn_{0.1}O_2$ cathode with high discharge capacity and rate performance for all-solid-state lithium battery, *J. Energy Chem.*, 2020, **40**, 39–45.
5 X. Cai, Z. Wang, Y. Xing, C. Zheng, P. Yan, W. Bao, T. Xie, Y. Hu, Y. Deng, Y. Zhang, Y. Wu, S. Yang, F. Zheng, H. Zhang, Z.-J. Wang and J. Xie, Promotion of the Nucleation of Ultrafine Ni-Rich Layered Oxide Primary Particles by an Atomic Layer-Deposited Thin Film for Enhanced Mechanical Stability, *Nano Lett.*, 2023, **23**(12), 5770–5778.
6 Y. Kim, C. Juarez-Yescas, D. W. Liao, M. K. Jangid, P. Joshi, H. Yang, B. Zahiri, P. V. Braun and N. P. Dasgupta, Thin Free-Standing Sulfide/Halide Bilayer Electrolytes for Solid-State Batteries Using Slurry Processing and Lamination, *ACS Energy Lett.*, 2024, **9**(4), 1353–1360.
7 H. Zhang, Z. Yu, J. Cheng, H. Chen, X. Huang and B. Tian, Halide/sulfide composite solid-state electrolyte for Li-anode based all-solid-state batteries, *Chin. Chem. Lett.*, 2023, **34**(11), 108228.
8 Y. Han, S. Jung, H. Kwak, S. Jun, H. Kwak, J. H. Lee, S.-T. Hong and Y. S. Jung, Single- or Poly-Crystalline Ni-Rich Layered Cathode, Sulfide or Halide Solid Electrolyte: Which Will be the Winners for All-Solid-State Batteries?, *Adv. Energy Mater.*, 2021, **11**, 2100126.
9 Y. Lee, J. Jeong, H. J. Lee, M. Kim, D. Han, H. Kim, J. M. Yuk, K.-W. Nam, K. Y. Chung and H.-G. Jung, Lithium argyrodite sulfide electrolytes with high ionic conductivity and air stability for all-solid-state Li-ion batteries, *ACS Energy Lett.*, 2021, **7**(1), 171–179.
10 J. Wang, S. Zhao, A. Zhang, H. Zhuo, G. Zhang, F. Han, Y. Zhang, L. Tang, R. Yang and L. Wang, High lithium-ion conductivity, halide-coated, Ni-rich NCM improves cycling stability in sulfide all-solid-state batteries, *ACS Appl. Energy Mater.*, 2023, **6**(7), 3671–3681.
11 M. Dubarry, N. Qin and P. Brooker, Calendar aging of commercial Li-ion cells of different chemistries – A review, *Curr. Opin. Electrochem.*, 2018, **9**, 106–113.
12 Y. Xiao, Y. Wang, S.-H. Bo, J. C. Kim, L. J. Miara and G. Ceder, Understanding interface stability in solid-state batteries, *Nat. Rev. Mater.*, 2020, **5**(2), 105–126.
13 W. Kim, J. Noh, S. Lee, K. Yoon, S. Han, S. Yu, K.-H. Ko and K. Kang, Aging Property of Halide Solid Electrolyte at the Cathode Interface, *Adv. Mater.*, 2023, **35**(32), 2301631.
14 J. D. McBrayer, M.-T. F. Rodrigues, M. C. Schulze, D. P. Abraham, C. A. Apblett, I. Bloom, G. M. Carroll, A. M. Colclasure, C. Fang, K. L. Harrison, G. Liu, S. D. Minteer, N. R. Neale, G. M. Veith, C. S. Johnson, J. T. Vaughey, A. K. Burrell and B. Cunningham, Calendar aging of silicon-containing batteries, *Nat. Energy*, 2021, **6**(9), 866–872.
15 J. Yun, H. R. Shin, T. D. Hoang, S. Kim, J. H. Choi, B. Kim, H. Jung, J. Moon and J.-W. Lee, Deciphering the critical degradation factors of solid composite electrodes with halide electrolytes: interfacial reaction versus ionic transport, *Energy Storage Mater.*, 2023, **59**, 102787.
16 M. C. Schulze, M.-T. F. Rodrigues, J. D. McBrayer, D. P. Abraham, C. A. Apblett, I. Bloom, Z. Chen, A. M. Colclasure, A. R. Dunlop, C. Fang, K. L. Harrison, G. Liu, S. D. Minteer, N. R. Neale, D. Robertson, A. P. Tornheim, S. E. Trask, G. M. Veith, A. Verma, Z. Yang and C. Johnson, Critical Evaluation of Potentiostatic Holds as Accelerated Predictors of Capacity Fade during Calendar Aging, *J. Electrochem. Soc.*, 2022, **169**(5), 050531.
17 Q. Ye, X. Li, W. Zhang, Y. Xia, X. He, H. Huang, Y. Gan, X. Xia and J. Zhang, Slurry-coated $LiNi_{0.8}Co_{0.1}Mn_{0.1}O_2$–$Li_3InCl_6$ composite cathode with enhanced interfacial stability for sulfide-based all-solid-state batteries, *ACS Appl. Mater. Interfaces*, 2023, **15**(15), 18878–18888.
18 C. Rosenbach, F. Walther, J. Ruhl, M. Hartmann, T. A. Hendriks, S. Ohno, J. Janek and W. G. Zeier, Visualizing the chemical incompatibility of halide and sulfide-based electrolytes in solid-state batteries, *Adv. Energy Mater.*, 2023, **13**(6), 2203673.
19 J. Cai, X. Zhou, T. Li, H. T. Nguyen, G. M. Veith, Y. Qin, W. Lu, S. E. Trask, M.-T. Fonseca Rodrigues, Y. Liu, W. Xu, M. C. Schulze, A. K. Burrell and Z. Chen, Critical Contribution of Imbalanced Charge Loss to Performance Deterioration of Si-Based Lithium-Ion Cells during Calendar Aging, *ACS Appl. Mater. Interfaces*, 2023, **15**(41), 48085–48095.
20 J. Cai, Z. Yang, X. Zhou, B. Wang, A. Suzana, J. Bai, C. Liao, Y. Liu, Y. Chen, S. Song, X. Zhang, L. Wang, X. He, X. Meng, N. Karami, B. Ali Shaik Sulaiman, N. A. Chernova, S. Upreti, B. Prevel, F. Wang and Z. Chen, Unveiling the parasitic-reaction-driven surface reconstruction in Ni-rich cathode and the electrochemical role of Li_2CO_3, *J. Energy Chem.*, 2023, **85**, 126–136.
21 S. Samanta, S. Bera, R. K. Biswas, S. Mondal, L. Mandal and A. Banerjee, Ionocovalency of the Central Metal Halide Bond-Dependent Chemical Compatibility of Halide Solid Electrolytes with Li_6PS_5Cl, *ACS Energy Lett.*, 2024, 3683–3693.
22 K. Andrikopoulos, A. Kalampounias, O. Falagara and S. Yannopoulos, The glassy and supercooled state of elemental sulfur: Vibrational modes, structure metastability, and polymer content, *J. Chem. Phys.*, 2013, **139**, 124501.
23 C. Nims, B. Cron, M. Wetherington, J. Macalady and J. Cosmidis, Low frequency Raman Spectroscopy for micron-scale and in vivo characterization of elemental sulfur in microbial samples, *Sci. Rep.*, 2019, **9**(1), 7971.
24 M. N. Ates, S. Mukerjee and K. M. Abraham, A high rate Li-rich layered MNC cathode material for lithium-ion batteries, *RSC Adv.*, 2015, **5**(35), 27375–27386.
25 L. Fang, M. Chen, K.-W. Nam and Y.-M. Kang, Redox Evolution of Li-Rich Layered Cathode Materials, *Batteries*, 2022, **8**(10), 132.
26 U. A. Stival, I. B. C. Gallo, C. F. N. Gonin, S. L. Reis, R. L. Grosso, J. B. Kosctiuk, M. G. S. Franchetti, B. Leão, F. E. R. Oliveira, A. Souza, H. R. Freitas, R. S. Monteiro, L. S. Parreira and M. A. C. Berton, Experimental challenges for electrochemical evaluation of cathodes in lithium-ion battery half-cells, *J. Energy Storage*, 2023, **72**, 108706.
27 T. Li, X.-Z. Yuan, L. Zhang, D. Song, K. Shi and C. Bock, Degradation Mechanisms and Mitigation Strategies of Nickel-Rich NMC-Based Lithium-Ion Batteries, *Electrochem. Energy Rev.*, 2020, **3**(1), 43–80.

28 D. H. S. Tan, E. A. Wu, H. Nguyen, Z. Chen, M. A. T. Marple, J.-M. Doux, X. Wang, H. Yang, A. Banerjee and Y. S. Meng, Elucidating Reversible Electrochemical Redox of Li_6PS_5Cl Solid Electrolyte, *ACS Energy Lett.*, 2019, **4**(10), 2418–2427.

29 L. Wang, X. Sun, J. Ma, B. Chen, C. Li, J. Li, L. Chang, X. Yu, T.-S. Chan, Z. Hu, M. Noked and G. Cui, Bidirectionally Compatible Buffering Layer Enables Highly Stable and Conductive Interface for 4.5 V Sulfide-Based All-Solid-State Lithium Batteries, *Adv. Energy Mater.*, 2021, **11**(32), 2100881.

30 Z. D. Hood, A. U. Mane, A. Sundar, S. Tepavcevic, P. Zapol, U. D. Eze, S. P. Adhikari, E. Lee, G. E. Sterbinsky, J. W. Elam and J. G. Connell, Multifunctional Coatings on Sulfide-Based Solid Electrolyte Powders with Enhanced Processability, Stability, and Performance for Solid-State Batteries, *Adv. Mater.*, 2023, **35**(21), 2300673.

31 A. Mills, S. Kalnaus, W.-Y. Tsai, Y.-F. Su, E. Williams, X. Zheng, S. Vaidyanathan, D. T. Hallinan Jr, J. Nanda and G. Yang, Elucidating Polymer Binder Entanglement in Free-standing Sulfide Solid-State Electrolyte Membranes, *ACS Energy Lett.*, 2024, **9**, 2677–2684.

